Australian Government
Department of Defence
Defence Science and
Technology Organisation

Design Methodology for Scarf Repairs to Composite Structures

C. H. Wang and A. Gunnion

Air Vehicles Division
Defence Science and Technology Organisation

DSTO-RR-0317

ABSTRACT

Scarf repairs are the preferred method of repairing thick composite structures, especially when externally bonded patches can no longer meet the stiffness, strength, and flushness requirements. Present designs of scarf repairs are based on two-dimensional analyses of scarf joints, assuming a uniform stress distribution along the scarf. This report presents an improve design methodology for designing scarf repairs to composite laminates. With the aid of elastic-plastic analyses, a critical assessment of the current design methods has been carried out, with major emphasis being placed on the stress/strain concentration along the bondline. It is proposed to replace the shear stress criterion with the maximum strain criterion. Comparison with experimental results confirmed that the new approach provides an improved first-order prediction of repair efficiency of scarf repairs.

RELEASE LIMITATION

Approved for public release

Published by

DSTO Defence Science and Technology Organisation
506 Lorimer St
Fishermans Bend, Victoria 3207 Australia

Telephone: (03) 9626 7000
Fax: (03) 9626 7999

AR-013-718
August 2006

APPROVED FOR PUBLIC RELEASE

Design Methodology for Scarf Repairs to Composite Structures

Executive Summary

Scarf repairs are currently the preferred method for repairing thick composite structures to restore the load-carrying capability to its as-designed level. Current design methodology, as codified in DEF (AUST) 9005, employs an analysis approach that is applicable to joints between isotropic materials (e.g., metallic structures). Several issues have been identified regarding the range of validity of the current approach. The purpose of the present investigation is to first critically assess the current design approach and to propose an improved design methodology that would remove un-necessary conservatisms of the current standard.

Elastic-plastic finite element analyses of scarf joints and scarf repairs have been performed to investigate the stress/strain concentration in composite-to-composite scarf joints and repairs, especially the influence of stacking sequence, laminate thickness, and adhesive yielding on the distribution of shear strain in the bondline. The analyses are then extended to three-dimensional scarf repairs, focusing on the load shedding phenomenon of scarf repairs, as the surrounding laminate provides multiple load paths. Based on the computational results, it is concluded that scarf repairs should be designed on the basis of a strain-based criterion. Comparison with experimental results confirmed that the new approach provides an improved first-order prediction of repair efficiency of scarf repairs.

The design approach proposed in this report represents a considerable improvement over the method in the RAAF's current design standard.

Authors

Chun H. Wang
Air Vehicles Division

Dr. Chun H. Wang is currently a Principal Research Scientist and the Head of the Composites and Low Observables Technology area in the Air Vehicles Division. Prior to joining DSTO in 1995, he has held various academic positions at the University of Sheffield, UK, the University of Sydney, and Deakin University, Australia. His main research experience is in the areas of advanced composite structures, repairs to metallic and composite structures, fatigue and fracture mechanics.

Andrew Gunnion
Corporate Research Centre in Advanced Composite Structures (CRC-ACS)

Dr Andrew Gunnion is a research engineer at the CRC-ACS, where he is currently working in several research fields including bird-strike analysis, crash simulation of composite joints and repair methods for composite structures. After successfully completing his PhD, Dr Gunnion continued to work with Airbus and CRC-ACS as an RMIT research fellow until joining the CRC-ACS in 2005.

Contents

1. INTRODUCTION 1

2. STRESS DISTRIBUTIONS IN SCARF JOINT 2
2.1 Elastic analysis 2
2.2 Elastic-plastic analysis 5

3. EXPERIMENTS AND RESULTS 11

4. ADHESIVE STRESSES IN SCARF REPAIRS 15

5. STRENGTH OF COMPOSITE ADHERENDS 19

6. STRAIN-BASED DESIGN METHOD FOR SCARF REPAIRS 23

7. CONCLUSIONS 25

1. Introduction

Scarf repairs are the preferred method of repair to restore the load-carrying capacity of a damaged composite structure to its as-designed strength. Current design methodology [1-3] recommends that a scarf repair should match, ply-by-ply, the original structure. With matched adherends, the adhesive stresses along the scarf are assumed to be uniform [4] and the joint is assumed to attain its maximum strength when the average shear stress reaches the ultimate shear strength of the adhesive.

For scarf joints between isotropic metallic adherends, the adhesive stresses are shown to be constant [5, 6]. Finite element analysis by Baker *et al* [7] confirmed that the shear stress along the scarf joint between adherends made of aluminium alloy is approximately constant, except near the free edges. However, significant stress concentrations have been found to exist in scarf joints between composite adherends of identical lay-up [7-9], with the maximum stresses occurring adjacent to the ends of 0° plies. The stress concentration factor depends strongly on the stacking sequence and thickness of the laminates. Since fibres themselves do not cross the bondline, the large stiffness disparity between the adhesive and the composite plies, especially 0° plies, induces significant stress variations along the scarf. In the case of brittle adhesives where joint strength is controlled by the maximum stress rather than the average shear stress, the current design methodology may significantly over-estimate joint strength, leading to potential premature failures. For ductile adhesives, strengths of scarf joints are limited by the maximum shear strain in the bondline. Although stresses would eventually become uniform as the adhesive undergoes plastic deformation, significant strain concentration may still occur. Consequently, the maximum strain in the adhesive bond may exceed the strain allowable before the *average* shear stress reaches the stress allowable. In this case, the current design methodology may be non-conservative. One major objective of this study is to assess the range of validity of the current design approach for scarf repairs to composite structures using elastic-plastic finite element modelling and mechanical tests.

For highly loaded advanced composite structures, taper angles ranging from 20:1 to 60:1 are often required to restore a damaged structure to its as-designed ultimate strength. So a considerable amount of sound material must be removed to form a large tapered hole, especially in the case of thick laminates. The current design methodology for scarf repairs recommends that the scarf angle be determined by analysing a scarf joint representing the most highly loaded section in a three-dimensional scarf repair. In doing so the beneficial effect of load bypass by the parent structure around the patch is neglected. Soutis and Hu [10] reported that the scarf joint analysis approach underestimated the strength of scarf patch repairs by more than 40%. It is worth noting that Soutis and Hu treated the laminate and the patch as homogeneous materials. It is not clear to what extent their findings may be affected by the variations of ply stiffness in actual composite laminate and composite patch. So, another objective of the present study is to assess the effect of load shedding on strength of scarf repairs, with a view to developing optimal scarf repair requiring minimal material removal.

This paper is structured as follows: Elastic-plastic finite element analysis of scarf joints is first presented to highlight the effects of stacking sequence, laminate thickness, and plastic yielding on the stress and strain concentrations in a scarf joint between orthotropic composite laminates. Then the analysis is extended to examine the strain concentrations in three-dimensional scarf repairs. To validate the analyses, a series of experiments has been carried out, involving stiff and quasi-isotropic laminates with matched and un-matched laminates.

2. Stress distributions in scarf joint

2.1 Elastic analysis

For a scarf repair as shown in Figure 1(a) the stresses in the bondline may vary with the location around the scarf, depending on the applied loads. For a unit strip in line with the principal load direction, x direction in the present case as shown by Figure 1(b), both the shear and peel stresses in the adhesive are assumed to be uniform and equal to the average values, τ_{av}, and σ_{av}, respectively. The average shear and peel stresses are related to the applied stress via the following expressions [6],

$$\tau_{av} = \frac{1}{2}\sigma_{xx} \sin 2\theta, \tag{1}$$

$$\sigma_{av} = \sigma_{xx} \sin^2 \theta. \tag{2}$$

For isotropic adherends, such as metallic materials, the above solutions have been confirmed to agree well with computational results [6]. For composite laminates, however, the adhesive stresses can vary significantly along the scarf, because the in-plane stiffness of a composite laminate varies in the through-the-thickness direction [3], while the adhesive layer has a constant stiffness. Consequently high stress concentrations would occur adjacent to the ends of 0^o plies [7], particularly for laminates containing unidirectional (tape) plies, where the variation in stiffness along the scarf is significant.

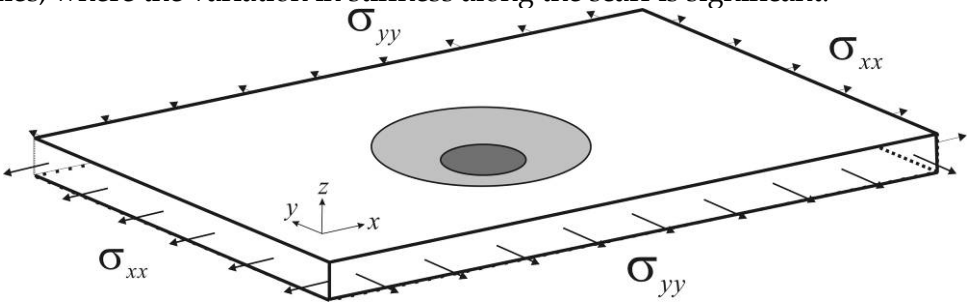

(a) A scarf repair subjected to biaxial stresses

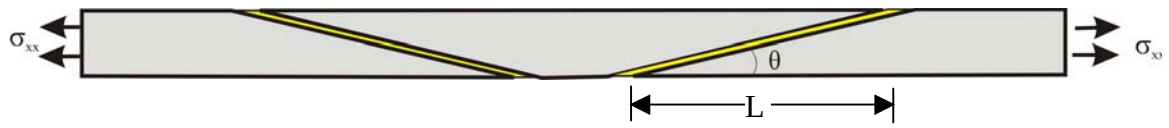

(b) An equivalent scarf joint

Figure 1 Structural models for (a) scarf repair and (b) representative scarf joint

To characterise the variation of adhesive stresses in a scarf joint between orthotropic composite laminates, finite element analyses were carried out. Four rows of elements were employed to model the adhesive, as illustrated in Figure 2. The properties of the composite material in the finite element model, presented in Table 1, were the same as in previous investigations [8, 9]. The shear modulus and Poisson's ratio of the adhesive were taken to be 390 MPa and 0.30, respectively. Quasi-isotropic laminates with a stacking sequence of $[45/0/-45/90]_{nS}$, where n equals to 1, 2, and 3, for three different laminate thicknesses, were modelled. The analysis used solid elements and was performed using MSC.Nastran.

Table 1 Properties of unidirectional composite laminar AS4-3501

E_{11}	$E_{22}=E_{33}$	ν_{12}	ν_{23}	$G_{12}=G_{13}$	G_{23}
128 GPa	13 GPa	0.3	0.3	7.2 GPa	5 GPa

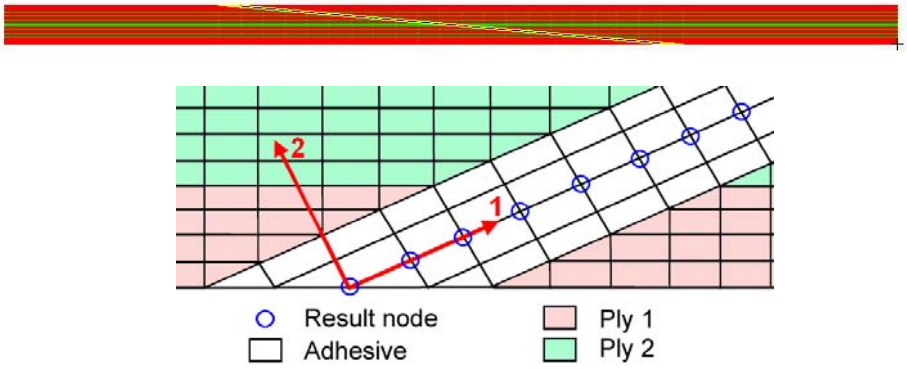

Figure 2 Finite element mesh near the bondline of a 5° scarf joint

Due to the mismatch in ply properties, there are many triple-point singularities where two adjacent plies intersect the adhesive. In the present investigation, the complex deformation at these singularity points will not be addressed. Instead, attention will be focused on the stresses and strains along the mid-plane of the adhesive layer, as depicted in Figure 2. This approach is equivalent to the stress-(or strain)-over-a-critical-distance method, with the distance being equal to half the bondline thickness. The normalised shear stress and peel stress are plotted in Figure 3, clearly showing the existence of significant stress concentrations in the bondline of a scarf joint between identical quasi-isotropic laminates. As expected, very high shear stresses occur at the ends of 0° plies. Even for moderately thick composite laminates of 32 plies, the maximum stress concentration factor exceeds 1.5. These stress concentrations may cause shear failure (if the maximum shear stress criterion is applied) at a load much lower than if the average shear stress criterion is used.

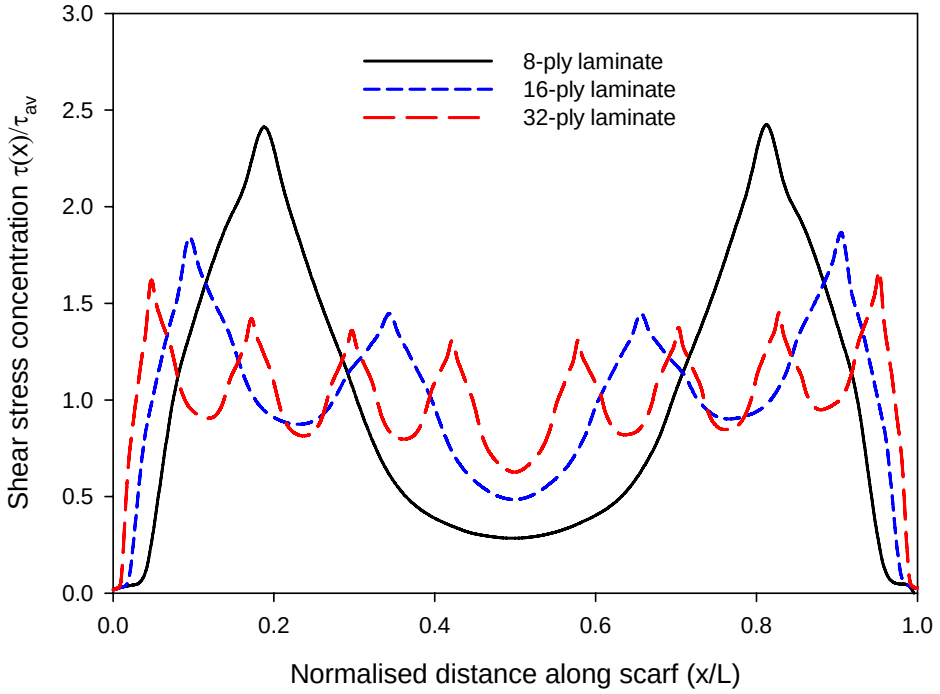

(a) Shear stress

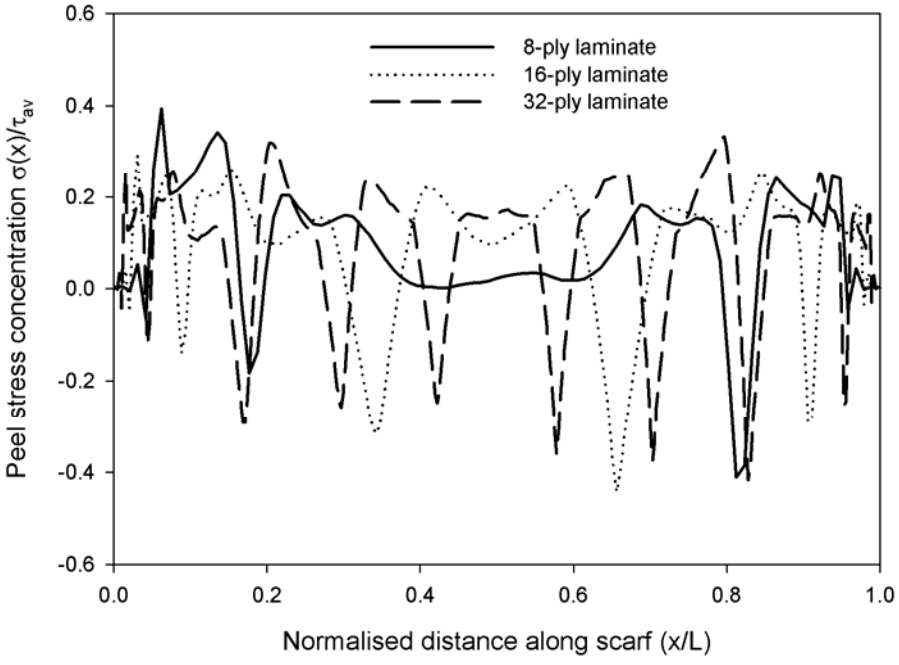

(b) Peel stress

Figure 3 Stress concentrations in a scarf joint ($\theta = 5^o$) between quasi-isotropic composite laminates. (a) Shear stress and (b) peel stress. Stacking sequences are respectively $[45/0/-45/90]_S$, $[45/0/-45/90]_{2S}$, $[45/0/-45/90]_{3S}$.

Since the majority of structural adhesives can deform plastically prior to failure, particularly under shear deformation, predictions based on elastic analyses may be overly conservative. Therefore, it is necessary to incorporate the elastic-plastic deformation behaviour of the adhesive in strength prediction. To this end, elastic-plastic finite element analysis is required to quantify the resulting stress redistribution as the adhesive undergoes plastic yielding. This will be described in the next section.

2.2 Elastic-plastic analysis

A generalised plane-strain model was developed using MSC.Marc to characterise the variation of adhesive stresses in a scarf joint between orthotropic composite laminates with an elastic-plastic adhesive. Various quasi-isotropic lay-ups representative of test specimens, i.e., $[0/45/-45/90]_{2s}$ and $[90/-45/45/0]_{2s}$, were investigated. For off-angle plies, such as 45° and -45° plies, the anisotropic properties are determined by transforming the orthotropic ply properties to the coordinate system of the FE model; details are provided in Appendix A. From previous investigations [9], these lay-ups were considered to represent the upper and lower bounds to the influence of stacking sequence (assuming a symmetric, balanced lay-up), with 0^o plies on the laminate surface expected to produce higher local stresses at the bevelled tips.

For the finite element analysis, an improved mesh was developed to reduce the number of elements, while maintaining sufficient resolution along the scarf. The mesh was optimised so that an equivalent mesh scheme could be implemented for the 3-D analysis (Section 4). Each ply is modelled by four rows of elements close to the bondline and by one row of elements away from the joint region. A portion of the finite element mesh is shown in Figure 4.

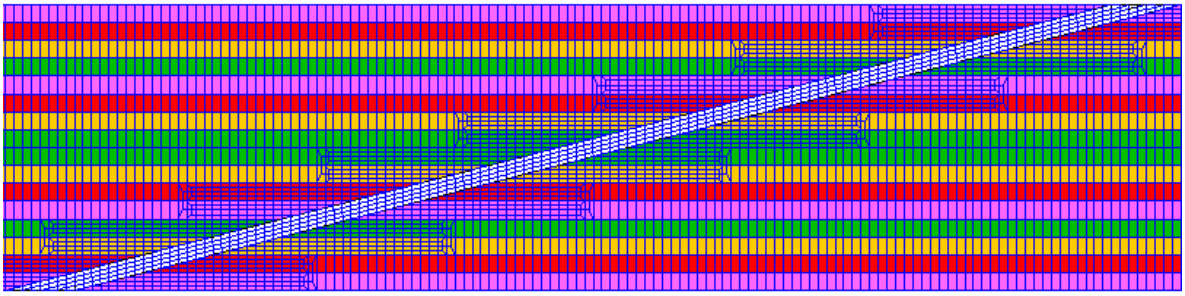

Figure 4 Finite element mesh near the scarf joint region

The scarf angle has a major effect on the average stress in a scarf joint, as indicated by equation 1. However, in the limiting case of very small scarf angle, the adhesive shear stress at each ply end is approximately proportional to the ply stiffness [3, 11], and is thus insensitive to the scarf angle. Therefore, an arbitrary scarf angle of 5° was chosen in the finite element analysis and the experiments described in Section 3. The ply properties were taken to match the experimental investigation and are given in Table 2. The ply thickness was assumed 0.2 mm, and equal to the bondline thickness. The total model length between boundary conditions was 100 mm, which is approximately three times the scarf length.

Table 2 Material properties unidirectional carbon fibre pre-preg: Cycom 970/T300 12K

E_{11}	$E_{22}=E_{33}$	ν_{12}	ν_{23}	$G_{12}=G_{13}$	G_{23}
120 GPa	8 GPa	0.45	0.02	5 GPa	2.7 GPa

Typical elastic-plastic behaviour for Cytec FM-300-2 epoxy adhesives [12] under a range of temperatures are presented in Figure 5. The adhesive strain has been truncated at unity (1.0). It is clear from Figure 5 that the adhesive becomes increasingly more ductile as the temperature increases. To simplify the computational analyses without compromising the applicability of the numerical results, the adhesive stress-strain curve is idealised to be elastic-perfectly plastic, as shown in Figure 6. With this idealisation, only two parameters are required to model the adhesive: the yield stress (τ_Y) and the ultimate shear strain (γ_F). Obviously both depend strongly on temperature. Although the shear moduli of structural adhesives are also dependent on temperature, their effects on adhesive stresses and strains are relatively minor and are not considered in this investigation.

The mechanical properties of film adhesive FM300 for both metallic and composite adherends can be found in Reference [13]. Based on these properties, the normalised ultimate shear strain (γ_F / γ_Y) is plotted versus temperature in Figure 7. Since the adhesive yield stress is far lower than the moduli of the adhesive and the composite adherend, the finite element results obtained for a reference temperature can be displayed in a non-dimensional form. The stresses and strains at any other temperature can be obtained by rescaling the reference results by the yield stress ratio. As a result, only one set of finite element analysis is required. In the present investigation, the reference temperature is chosen to be room temperature. The pertinent shear modulus, Poisson's ratio, and yield stress of the adhesive are equal to 840 MPa, 0.35, and 50 MPa, respectively.

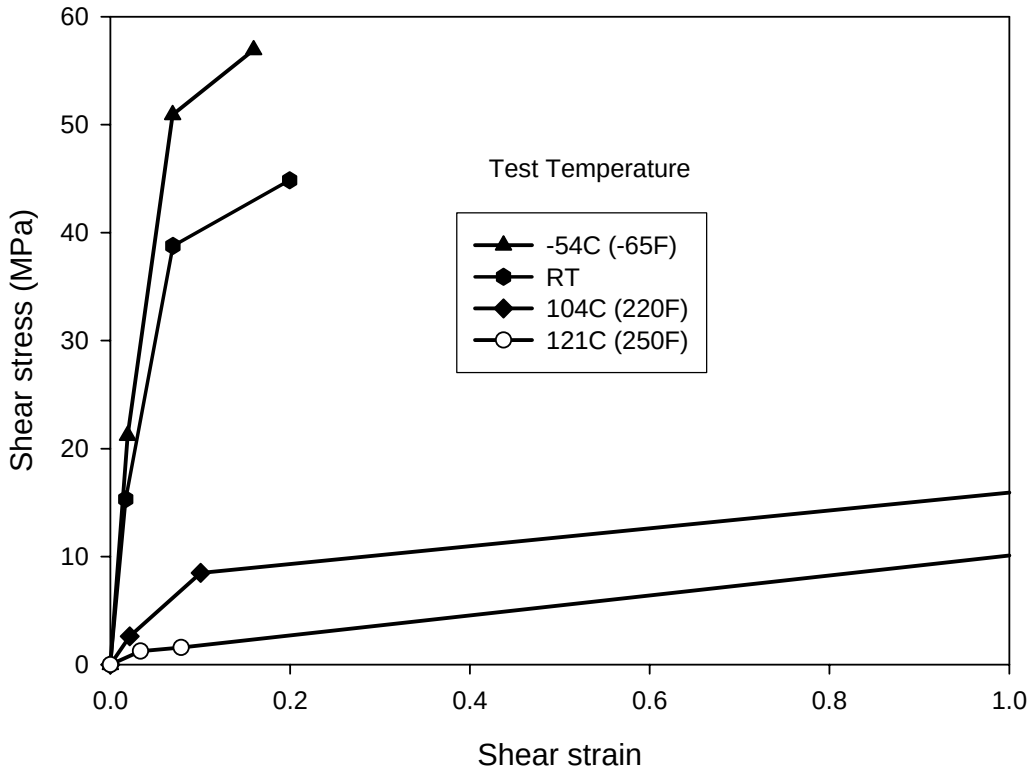

Figure 5 Shear stress versus shear strain of FM 300-2 film adhesives. Data are taken from Reference [12].

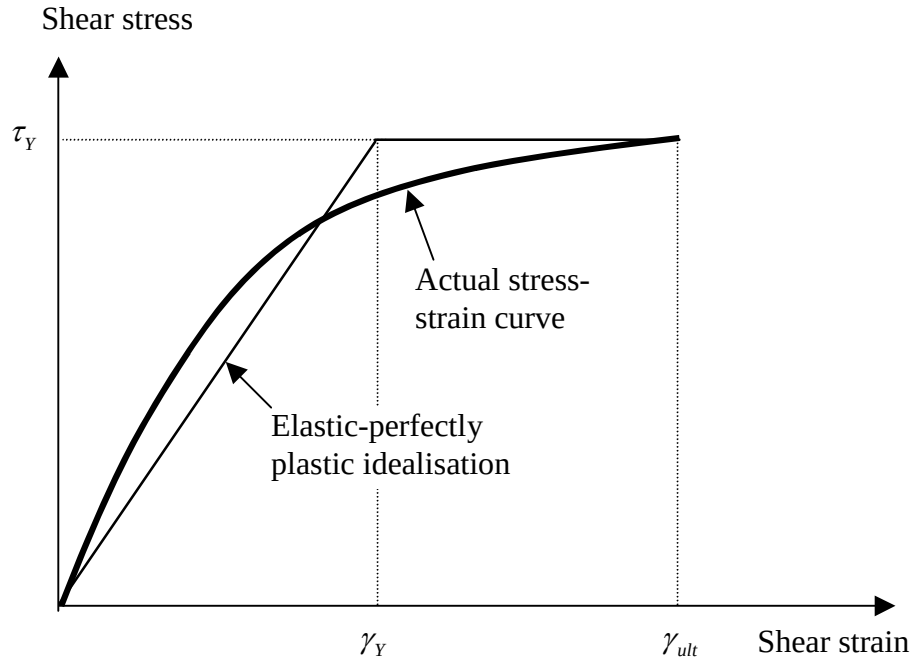

Figure 6 Elastic-perfectly plastic idealisation of adhesive shear stress-strain relationship

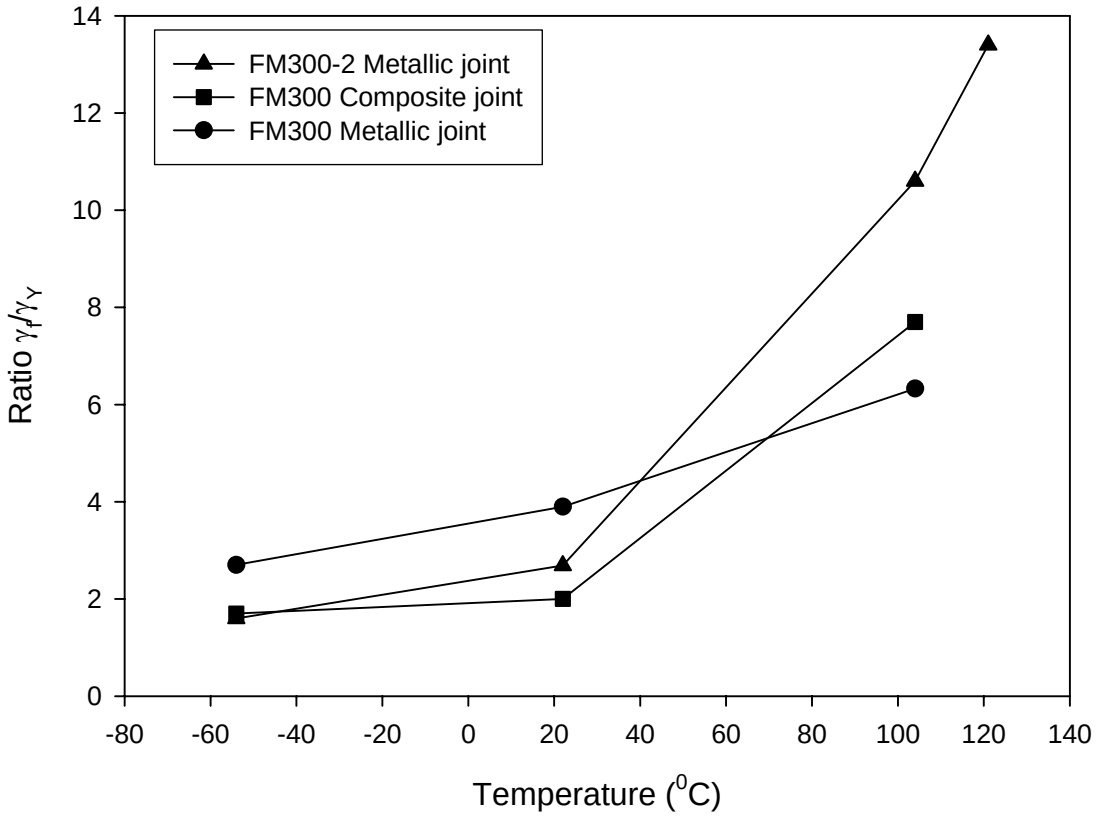

Figure 7 Ratio between ultimate shear strain and yield strain for FM300 adhesive

From the results of an incremental elastic-plastic analysis, the normalised shear stress, τ_{av}/τ_Y, along the bondline is shown in Figure 8. It is clear that as the applied load increases the shear stress approaches the yield stress over the entire scarf. By contrast, the shear strain, as shown in Figure 9, remains highly concentrated near the ends of 0° plies. However, at a given applied load or average shear stress, the adhesive bonds in both lay-ups experience a similar level of peak shear strain, as shown in Figure 10. The significance of the results presented in Figure 10 is that if the failure of adhesive in a scarf joint is solely dependent on the maximum shear strain, then the computational results suggest that the joint strength would be insensitive to the laminate stacking sequence. To verify this prediction, experiments were carried out and the results are presented in the next section.

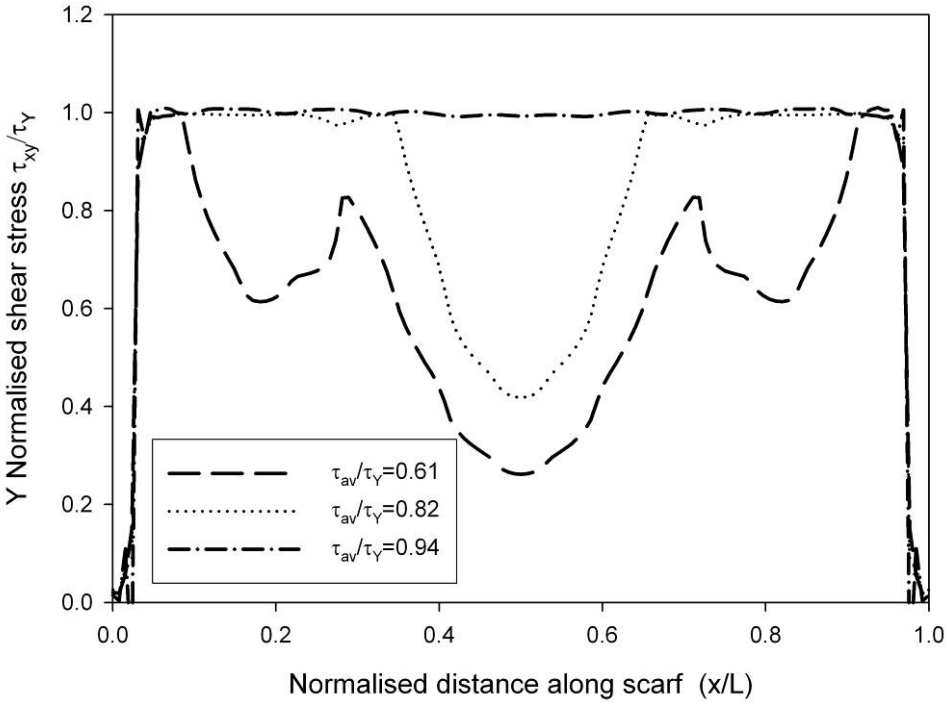

(a) $[0/45/-45/90]_{2s}$

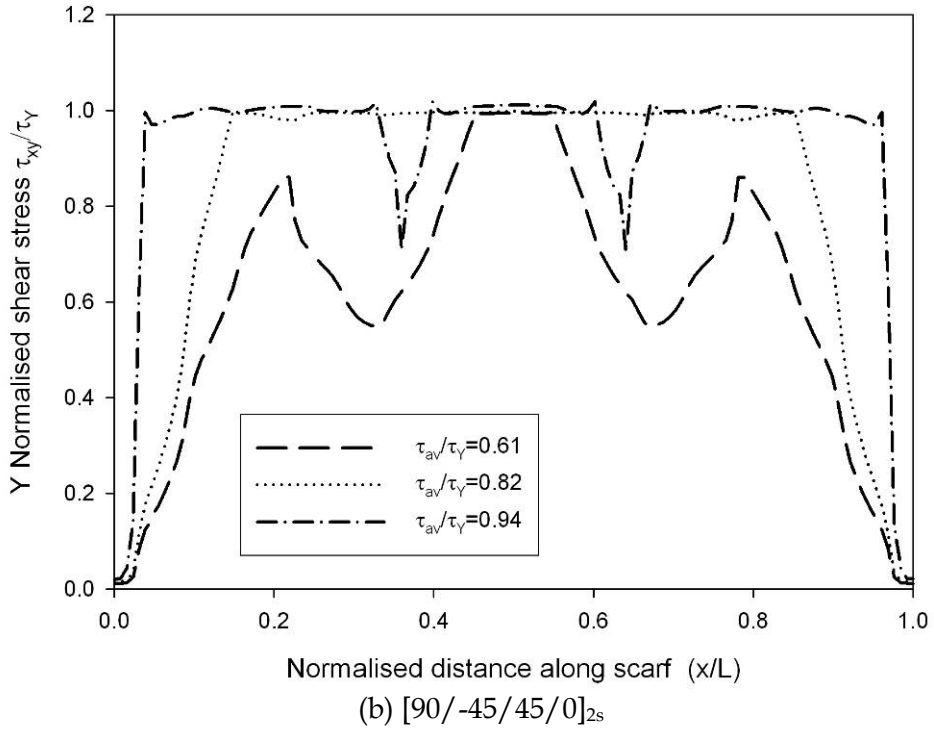

(b) $[90/-45/45/0]_{2s}$

Figure 8 Shear stress distribution (shear stress normalised by yield stress, loading indicated by average shear normalised by yield stress) for (a) $[0/45/-45/90]_{2s}$ and (b) $[90/-45/45/0]_{2s}$

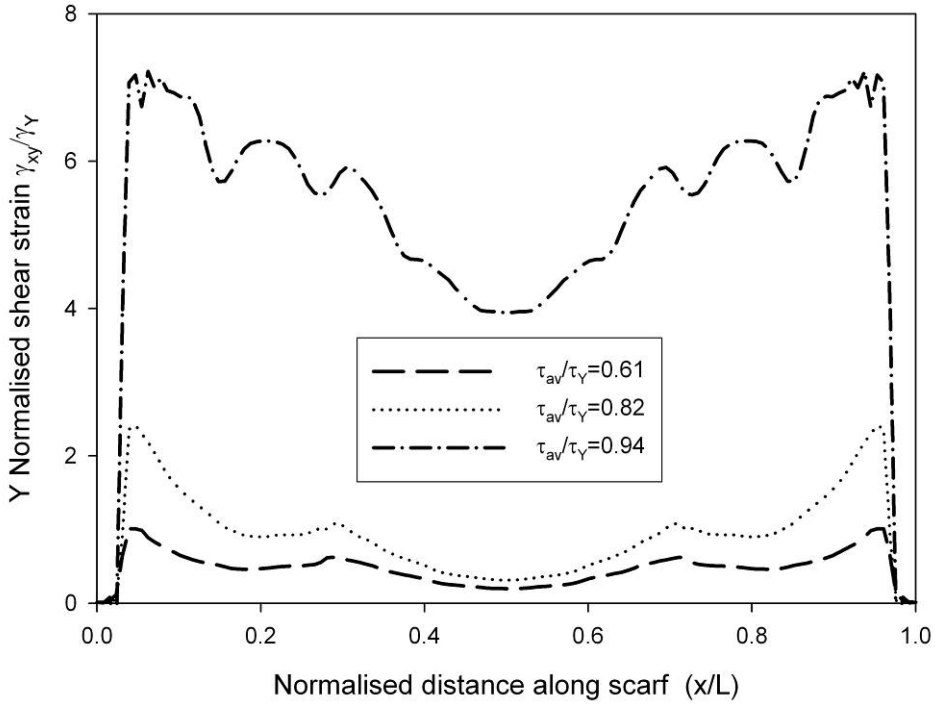

(a) $[0/45/-45/90]_{2s}$

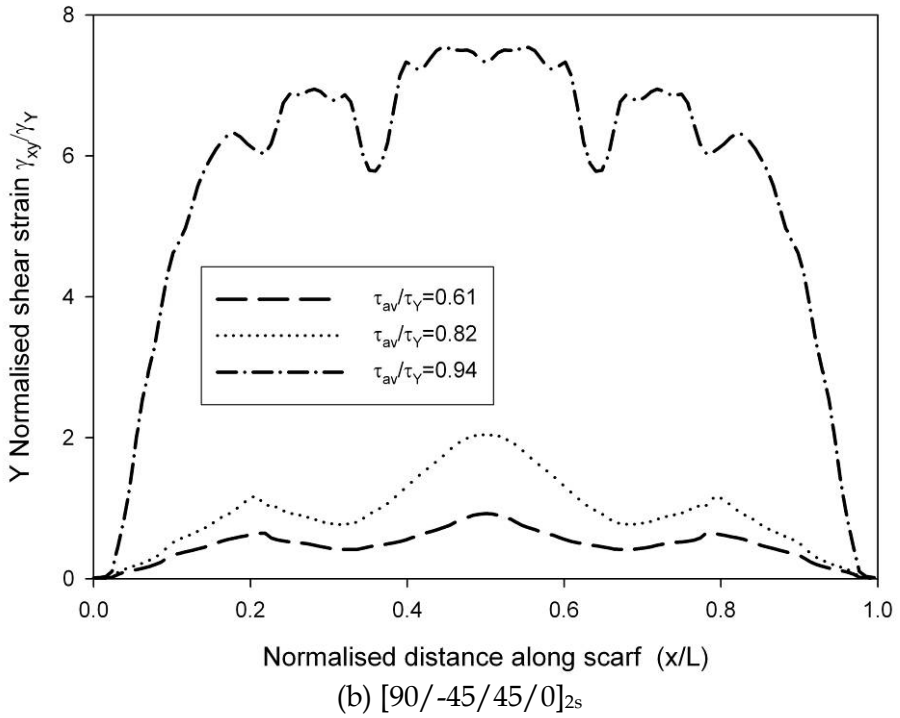

(b) $[90/-45/45/0]_{2s}$

Figure 9 Shear strain distribution along scarf (shear strain normalised by yield strain for (a) $[0/45/-45/90]_{2s}$ and (b) $[90/-45/45/0]_{2s}$

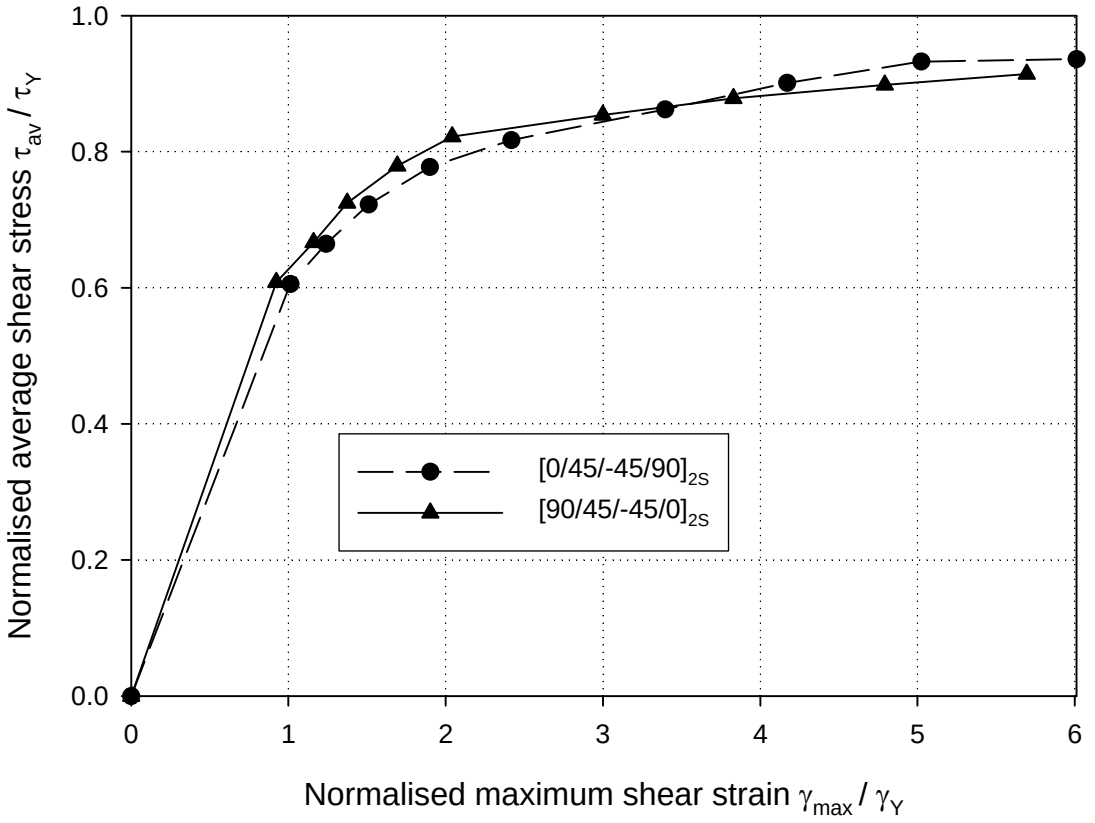

Figure 10 Average shear stress versus maximum shear strain for two different stacking sequences.

3. Experiments and Results

Three different types of scarf joints were selected to assess the influences of adherend stiffness and stacking sequence on joint strength. All specimens had identical scarf angle of 5° and identical width of 25 mm. The first joint type comprised of metallic adherends (aluminium 2024-T3, thickness = 3 mm) bonded with FM300 film adhesive, while the second set of specimens were made of 21-ply orthotropic laminates (T300/914C) bonded with FM300-2K adhesive [14]. The stacking sequence of the 21-ply composite laminate is $[45/-45/90/0_3/45/0_2/-45/\overline{90}]_S$.

For the third set of specimens, 16-ply laminates with two different stacking sequences (laminate A with a stacking sequence of $[0/45/-45/90]_{2s}$ and laminate B having a stacking sequence of $[90/-45/45/0]_{2s}$) were made of IM7/977-3 carbon/epoxy prepregs. Three different joints with either of the two laminates were bonded with FM300-2K adhesive:

joints between (i) laminate A and laminate A (denoted as 0-0 joint), (ii) laminate A and laminate B (denoted as 0-90 joint), and (iii) laminate B and laminate B (denoted as 90-90 joint).

All specimens were loaded in tension until failure. Based on the measured failure load, the average shear stress is calculated using equation (1). For the metallic scarf joints, the average bondline shear stresses at failure for three specimens was approximately 38 MPa, which compares very well with the adhesive strength (35 MPa) obtained by the adhesive manufacturer using thick adherend shear tests (KGR-1 data) [15]. The good correlation between the adhesive shear strength from the two different test coupons is primarily due to the uniformity of shear stress along both types of joints.

For the second series of specimens, scarf joints between 21-ply composite laminates bonded with FM300-2K adhesive, the average shear stress at failure was approximately 32 MPa. According to the manufacturer data sheet, the lap shear strength of FM300-2K is close to 45 MPa at room temperature [16]. Therefore, the ratio of average shear stress to ultimate shear stress of the adhesive is close to 0.71. For comparison, the present model predicts that the ratio should be close to 0.82, referring to Figure 10, since the ratio of γ_F / γ_Y for FM300-2K at room temperature is approximately 2.5. The discrepancy between the experimental results and the model prediction could be attributed to two factors. Firstly, adhesive bonding of composite adherends whose fibres have been exposed by the machining operation may not achieve the same level of strength as bonding between metallic adherends. Secondly, the results presented in Figure 10 are for scarf joints between quasi-isotropic laminates, hence some minor difference may exist between the 21-ply stiff laminate and quasi-isotropic laminates.

For the third series of specimens, composite scarf joints between 16-ply quasi-isotropic laminates bonded using FM300-2K adhesive, the ratio between average shear and yield strength varied between 0.62 and 0.9, as plotted in Figure 11. Since the ratio of the adhesive (FM300-2K) ultimate shear strain to the yield strain is approximately equal to 2.5 at room temperature, as shown in Figure 7, the predicted joint strength based on the FE results (Figure 10) is approximately equal to 0.82, which is included in Figure 11. Two important observations can be made. Firstly, joints between composite adherends 90° surface plies are stronger than joints between adherends featuring 0° surface plies. Secondly, the model prediction is in reasonable agreement with the mean value of experimental results for the 90-90 scarf joints. However, the prediction overestimates the strengths of the other two types of joints, especially the 0-0 joint.

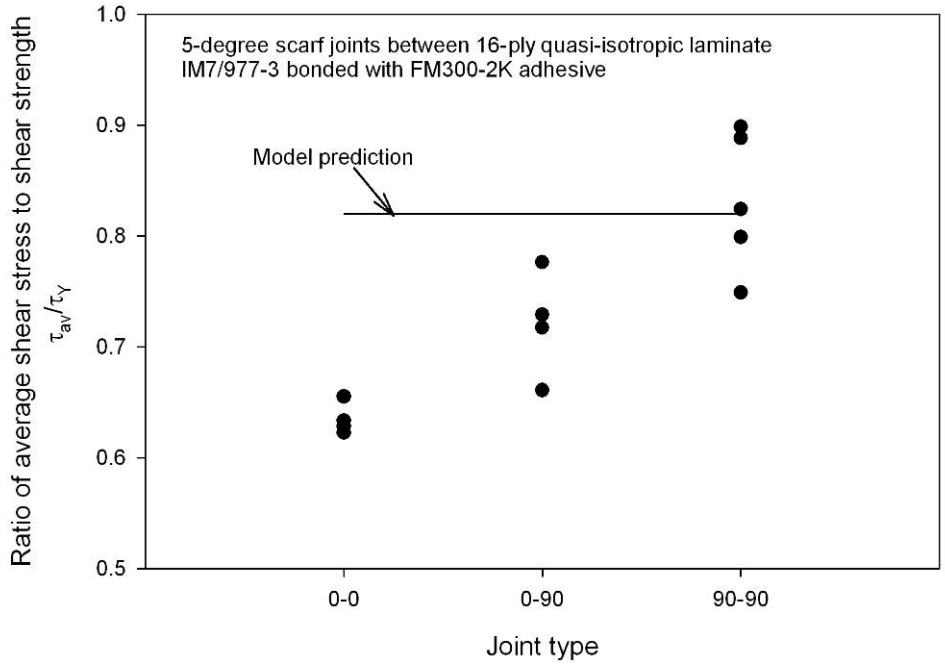

Figure 11 Average shear stresses in scarf joints at failure

One possible factor contributing to the over-prediction of the strengths of 0-0 and 0-90 joint types is the high strain concentration at the ends of 0° surface plies, which is not captured by the shear strain along the mid-plane of the adhesive layer. This is illustrated by the contour plots of shear strains in Figure 12 for two joint types, 0-0 and 90-90, at the onset of plastic yielding. Both specimens were loaded to the same maximum shear strain (along the mid-plane of the adhesive layer) of 0.06. It can be seen that for the 90-90 joint type the shear strain is uniformly distributed along the scarf and is constant through the adhesive thickness. However, for the 0-0 joint type a high localised shear strain exists at the tip of the surface ply (0° ply). Due to the free edge effect, the corner between the 0° ply and the adhesive along the specimen surface represents a singularity point. While the von Mises stress is bounded by the adhesive yield stress, the strains can be un-bounded and depend strongly on the finite element mesh size near the corner point. The significant differences between the strains in the 0-0 and 90-90 joint types are consistent with the observed failure modes for these two types of joints. As shown in Figure 13, the 0^0 surface ply in the 0-0 joint remain intact after joint failure, whereas the 90^0 surface ply and the sub-surface 45^0 ply in the 90-90 joint type clearly fractured, indicating that failure might have initiated close to the internal 0° plies, resulting in eventual overloading of the adherend tips.

The comparison between model prediction and experimental data shown in Figure 11 suggests that the maximum shear strain failure criterion provides an improved first order prediction. However, further improvement is required to capture the effect of corner singularities pertinent to the 0-0 type joint. This will be the subject of future work.

Nevertheless, the lower joint strength exhibited by the 0-0 type scarf joint implies that it is important to avoid the surface plies of scarf repairs being parallel to the major applied load.

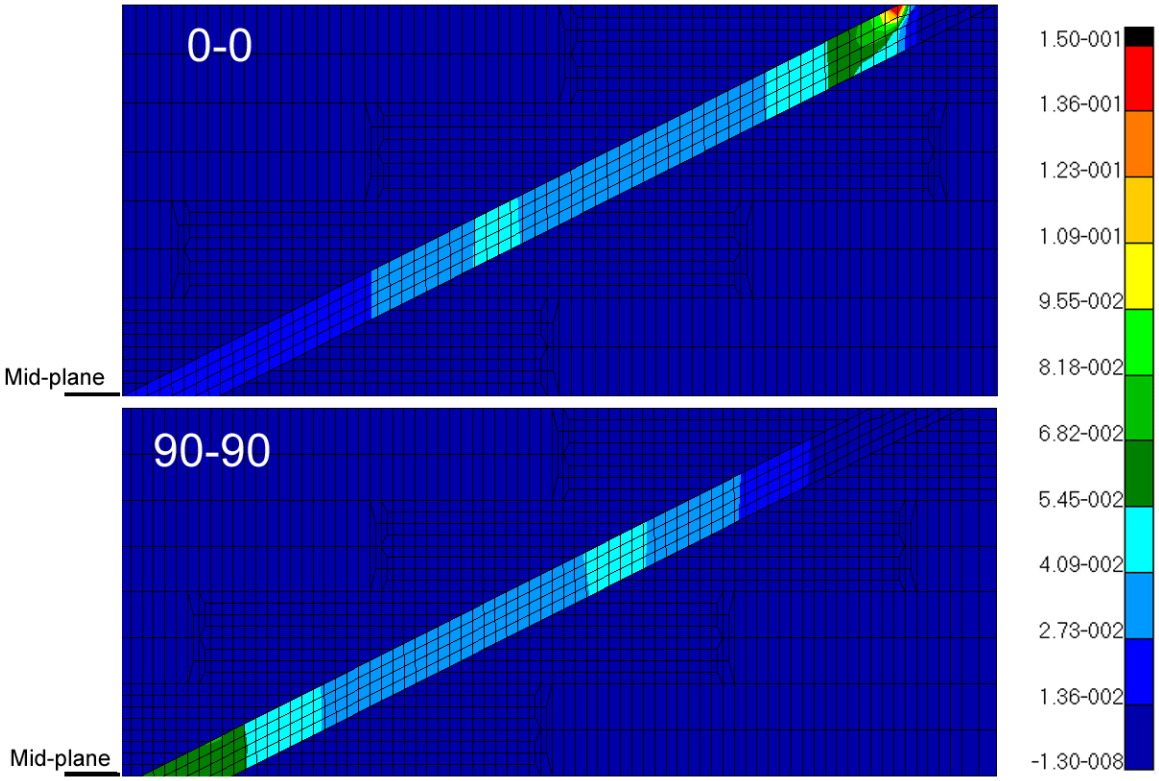

Figure 12 Localised strain singularities in scarf joint between orthotropic composite laminates

(a) Zero degree outer ply (b) 90 degree outer ply

Figure 13 Failure modes of (a) 0-0 and (b) 90-90 joint types.

4. Adhesive stresses in scarf repairs

Scarf joints, referring to Figure 1(b), are over simplified representations of scarf repairs, as all loads in a scarf joint are transferred through the adhesive bond. With scarf joints being single load-path structures, their maximum load carrying capacities are limited by the plastic collapse load of the adhesive bond, especially under hot/wet conditions when adhesives are ductile and have low shear strengths. For scarf repairs, referring to Figure 1(a), however, loads may be diverted around the repair when the adhesive undergoes plastic deformation. One possible consequence of this load shedding phenomenon is a lower average shear strain in the adhesive bond than in the equivalent scarf joint subjecting to the same applied stress. This implies that scarf repairs may afford a higher strength than the equivalent 2-D scarf joint. Soutis and Hu [10] reported that the 2-D scarf joint analysis underestimated the strength of the scarf patch repair by more 40% when adherend failure limits the joint and repair strengths. This difference was attributed to the stress redistribution in the repaired region due to the plastic deformation of the adhesive. It is worth pointing out that Soutis and Hu treated the composite adherends as being homogeneous, with elastic properties being equal to the laminate properties. Therefore the varying stiffness through the laminate thickness was not considered. It is, therefore, not clear whether the same is true for composite adherends where significant stress concentrations exist.

A finite element model was developed to characterise the variation of adhesive stresses in a three-dimensional scarf repair to an orthotropic composite laminate with an elastic-plastic adhesive. A circular scarf repair with a scarf angle of 5° is analysed. The mesh used for the elastic-plastic analysis was swept in an arc to produce the circular scarf, thus guaranteeing consistent mesh resolution around the adhesive for the two- and three-dimensional elastic-plastic analyses. A quarter of the finite element mesh is shown in Figure 14. The repair had lower and upper radii of 25 and 62 mm, respectively. The square panel had a half-width 300 mm. Hence, the panel can be considered sufficiently large with respect to the repair for this analysis, with $W/D \approx 5$.

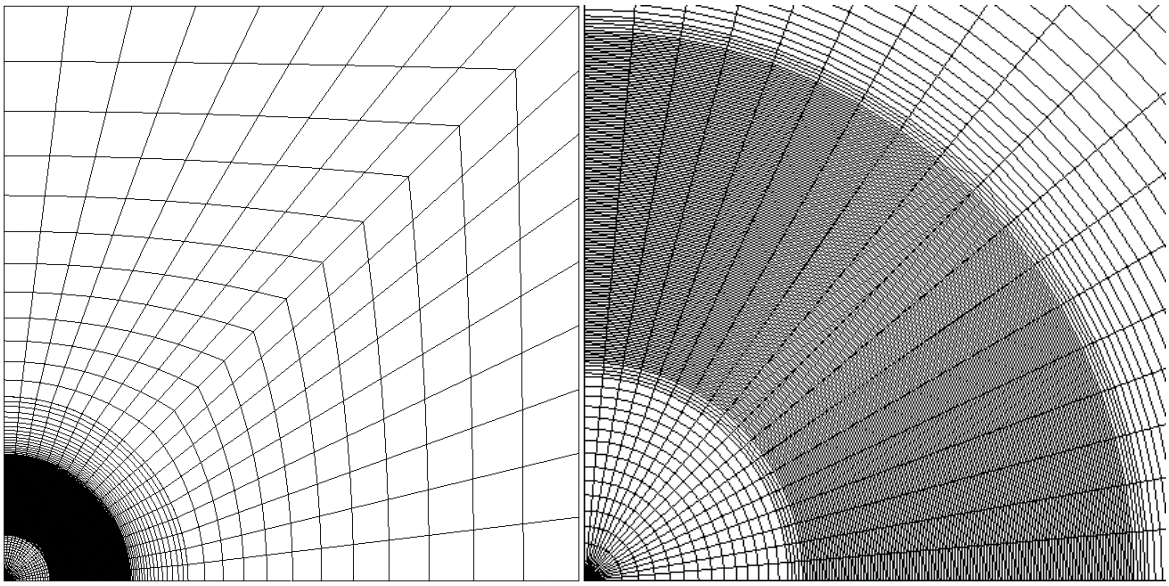

(a) One quarter of the entire panel (b) Refined region

Figure 14 Finite element mesh for a three-dimensional scarf repair

The same composite, adhesive and laminate properties were used as in the two-dimensional elastic-plastic analysis. The analysis methodology applied to the two-dimensional joint was repeated and the results are presented in Figure 15. The adhesive stresses and strains for the three-dimensional model were taken in the 0° (loading) direction. It is interesting to note that the difference between the two-dimensional joint and three-dimensional repair is only of the order of 10% at the elastic limit and close to zero at the high plastic strain limit. This result is rather unexpected, considering that the large difference between two-dimensional scarf joint and three-dimensional scarf repair reported by Soutis and Hu [10]. Further computational and experimental investigations are required to confirm the present finding that 2-D scarf joint analysis would provide a good prediction of the strength of three-dimensional scarf repairs.

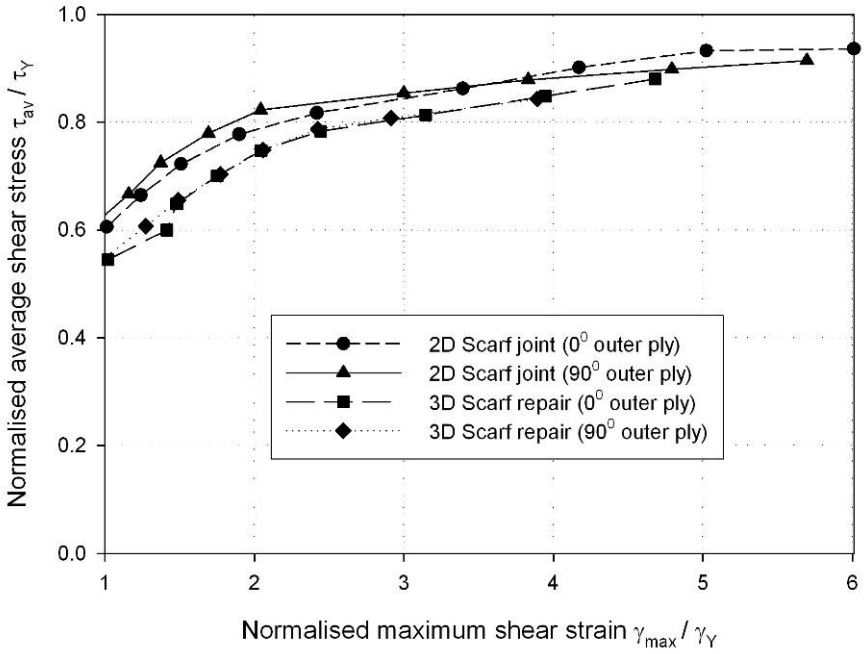

Figure 15 Average shear stress versus maximum shear strain for scarf repair at the highest load location

The normalised shear stress and the normalised shear strain along the radial line that is parallel to the loading direction are shown in Figure 16 and Figure 17. Comparison with the results pertinent to the representative scarf joint, as shown in Figure 8a and Figure 9a, reveals that the difference between scarf joint and scarf repair is very minor. This finding is again rather surprising, since Soutis and Hu [10] reported that a scarf repair could be as much as 400% stronger than the representative scarf joint for adhesive failure at high scarf angle. Even at low scarf angle when joint or repair strength is dominated by adherend failure, a scarf repair was reported to be around 40% stronger than the representative scarf joint [10]. To ascertain the differences between the strength of composite laminates in two-dimensional scarf joints and three-dimensional scarf repairs, a detailed comparison between the strains near the bevelled edges will be presented in the next section.

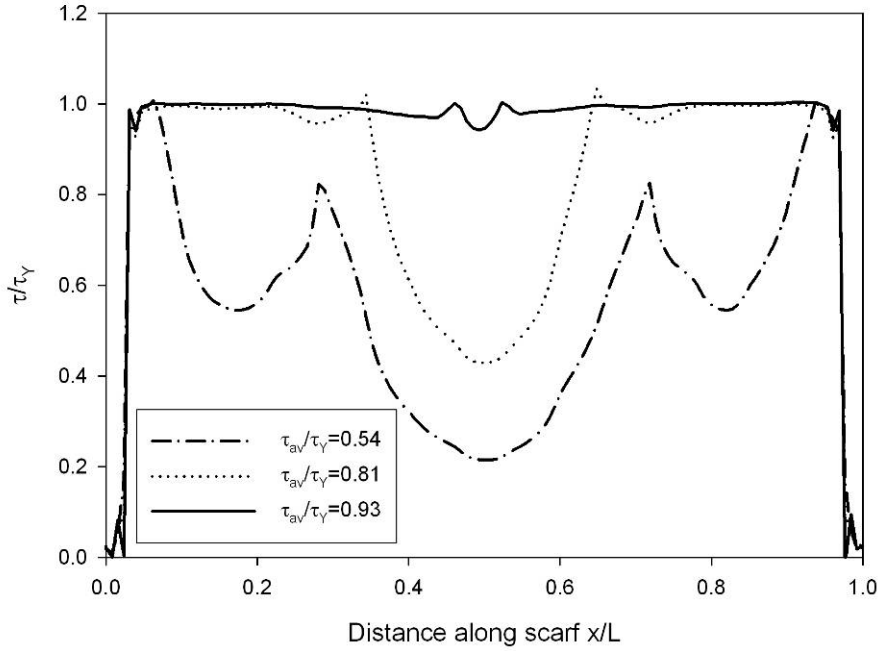

Figure 16 Shear stress distribution along 3-D scarf (shear stress normalised by yield stress for $[0/45/-45/90]_{2s}$)

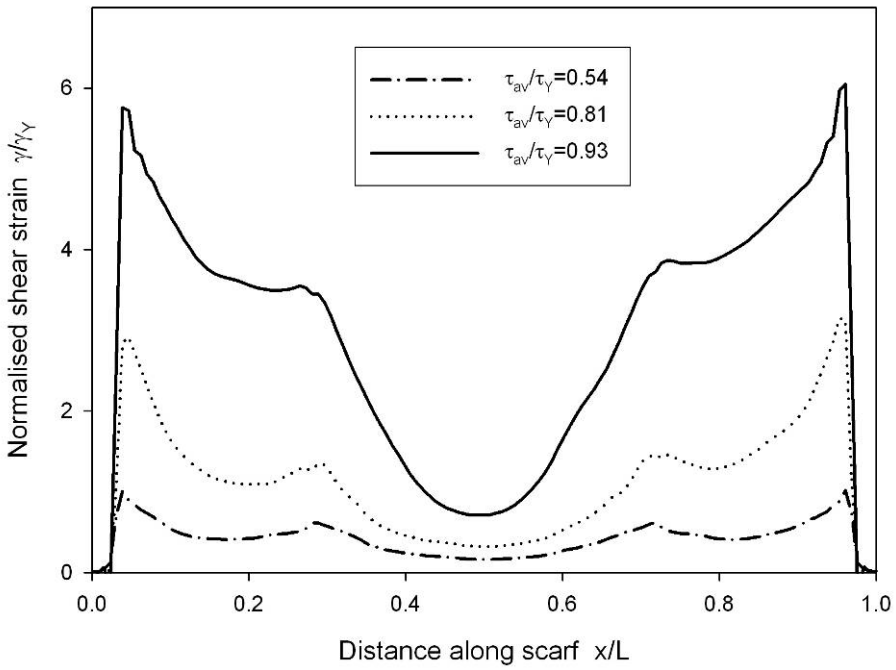

Figure 17 Shear strain distribution along 3-D scarf (shear strain normalised by yield strain for $[0/45/-45/90]_{2s}$)

5. Strength of Composite Adherends

One major consideration in designing scarf repairs is the potential failure of the composite adherends. Since both the parent laminate and the scarf patch have bevelled edges, it is important to avoid fracture of the feathered tips, due to high stress concentrations. The failure modes of the 0-0 joint (both adherends have 0° surface plies) and the 90-90 joint (both adherends have 90° surface plies), as illustrated in Figure 13a and Figure 13b, seem to suggest that failure initiated in the adhesive bond, probably close to the ends of 0° plies. Supporting the idea of failure started in the adhesive near the ends 0° plies is the relative low strain concentration in the composite adherends, as shown in Figure 18. Due to the strain singularities at corners where two adjacent plies meet the adhesive, the magnitude of the von Mises strain indicated in Figure 18 is only a qualitative indication of the length scale over which corner singularity prevails. The FE results suggest that joints with surface plies being parallel to the applied load exhibit a higher level of strain than joints whose surface plies are perpendicular to the applied load. Furthermore, the tip region of the 90-90 joint seems to experience a weaker singularity than the 0-0 joint. However, due to the relatively low stiffness of the first three plies near laminate surface, the tip region of the 90-90 joint experiences an elevated strain over a larger area than the 0-0 joint. This higher level of strain might have contributed to the observed breakage of the laminate displayed in Figure 13b. For comparison, the strain concentration contours of scarf repairs are shown in Figure 19.

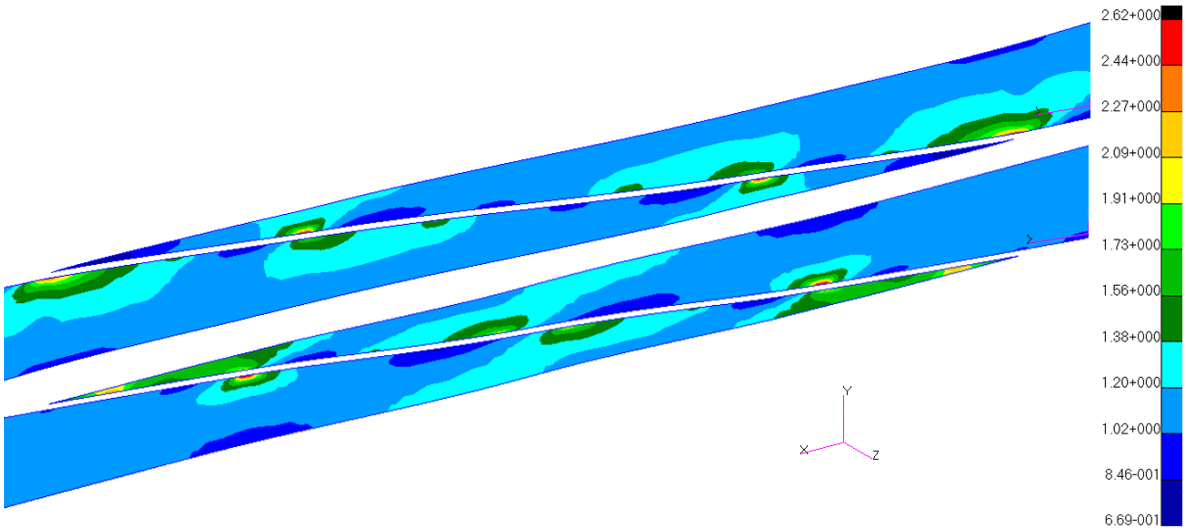

Figure 18 Ratios of laminate von Mises strain to applied strain for scarf joints with 0° surface ply (upper image) and 90° surface ply (lower image) under elastic conditions.

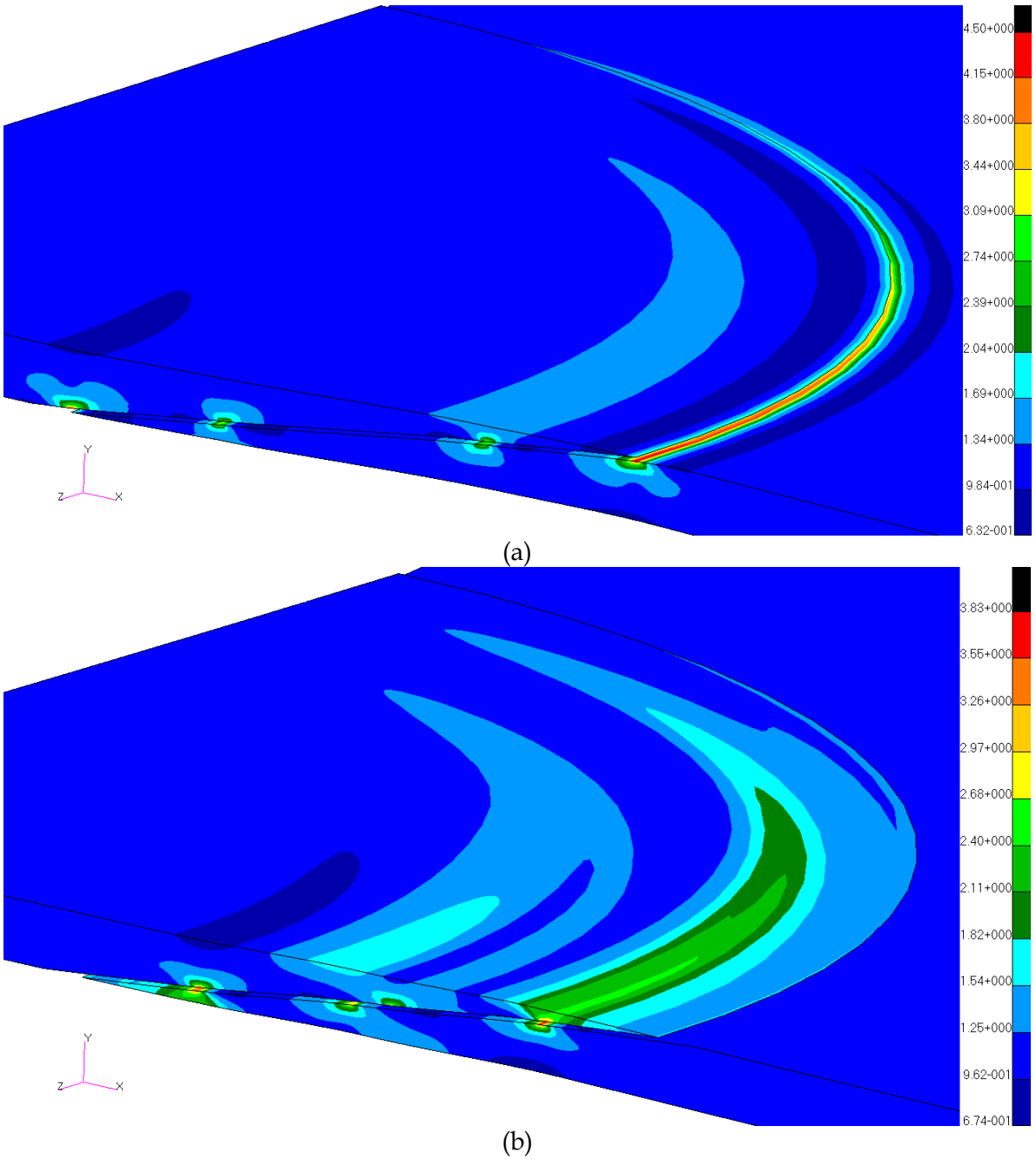

Figure 19 Concentrations of von Mises strain in scarf repairs with (a) 0° surface ply and (b) 90° surface ply.

Due to the extremely localised nature of the strain singularities in the composite laminates shown in Figure 18, a fracture-mechanics type of approach would be required to quantify the order and strength of the singularities at acute-angle corners. In the absence of proven fracture-mechanics based failure criteria for such problems, the point stress at a critical distance approach [17] will be employed to assess the significance of the three-dimensional effect of scarf repairs and the adequacy of the scarf joint analysis. The strain-invariant [18, 19] parameters, including the first strain invariant and the von Mises strain, are taken

along a vertical path (perpendicular to the applied load) radiating from the highest singularity point, as illustrated in Figure 20. The results for both 0-0 and 90-90 scarf joints and scarf repairs are presented in Figure 21. The distance is normalised by the ply thickness of the composite, while the strain invariant parameters are normalised by the respective applied values, i.e., the invariant values remote from the scarf.

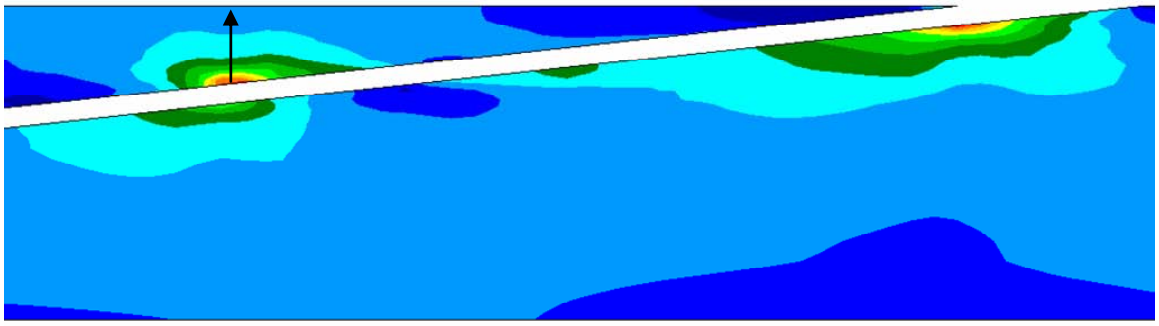

Figure 20 Tip fracture path, indicated by the arrow, for composite laminates of 0-0 joint.

It is apparent from Figure 21 that the composite adherends of a scarf repair experience a similar level of strain as the composite adherends in the equivalent scarf joint. This confirms that the two-dimensional scarf joint analysis is sufficiently accurate for the purpose of designing scarf repairs.

Generally the critical distance is a fitting parameter that must be obtained by experiment. However, a number of studies have suggested that the critical distance could be taken to be one-ply thickness [20, 21] or two-ply thicknesses [10]. In the present study, one-ply thickness will be employed as the critical distance to provide a quantitative comparison between scarf joints and scarf repairs. It can be seen from Figure 21 that the von Mises strain is approximately 1.52 times the applied value. This means that tensile fracture of the tips of the composite laminates will not occur as long as the strength of scarf joint is less than 66% of un-notched strength of the composite laminates. The present finding is supported by the experimental results of Pipes *et al* [22] in that scarf joint strength did not increase without limit as the scarf angle was made smaller. The highest scarf joint efficiency was found to be around 0.64 [22], which compares very well with the prediction of 0.66 by the present analysis. By contrast, due to the slightly higher strains experienced by the laminates in scarf repairs, tensile fracture of the laminate tips may occur at around 60% the un-notched strength.

With most carbon fibre laminae having failure strains exceeding 13,000 microstrains, scarf joints and scarf repairs can be respectively designed to strengths above 8580 and 7670 microstrains, without overloading the composite adherends. As an example, consider the IM7/5250-4 BMI/carbon composite material. Its un-notched laminar strength is close to 14,000 microstrains. This means that scarf joints and scarf repairs can be expected to sustain 9200 and 8235 microstrains, respectively, without failure in the composite laminates. The present results suggest that for composite structures that are designed to operate at less than 60% the un-notched strength, it suffices to consider only the adhesive

strength in designing scarf repairs. Given that typical maximum strain values used in aircraft composite repairs are around 5000 microstrains (accounting for environmental conditioning, impact damage or other stress concentrations) [23], this limit would encompass the majority of composite aircraft structures currently in service.

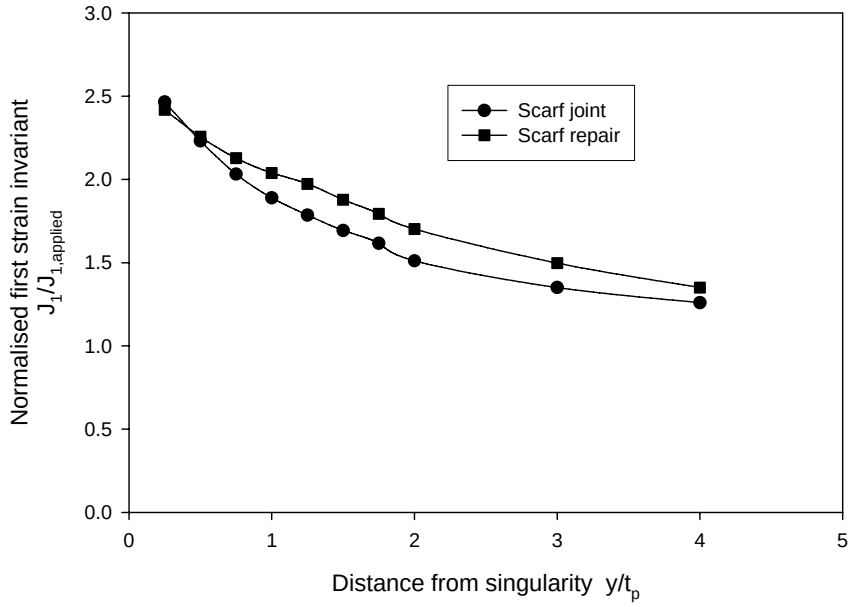

(a)

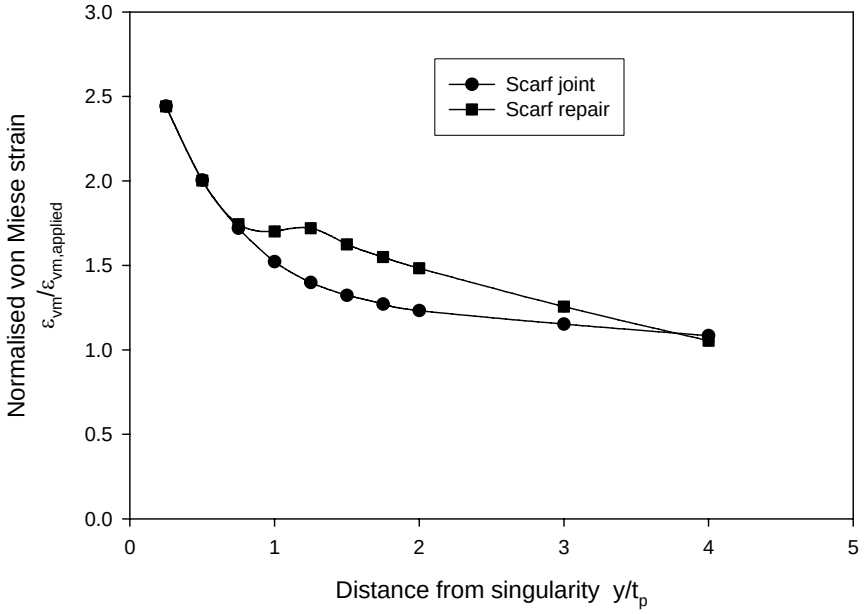

(b)

Figure 21 Concentration of strain-invariant parameters near the bevelled tips of composite laminates in 0-0 scarf joint and scarf repair; (a) first strain invariant and (b) von Mises strain

6. Strain-based design method for scarf repairs

The computational results of the finite element analysis revealed that the stacking sequence of the composite laminate has negligible effect on the maximum shear strain (along the mid-plane of the adhesive layer) for a given average stress. The numerical results presented in Figure 22 can be described by the following rational function,

$$\frac{\tau_{av}}{\tau_Y} = g(\frac{\gamma_{\max}}{\gamma_Y}), \tag{3}$$

with

$$g(x) = 1 - \frac{\alpha}{x+\beta}, \tag{4}$$

where the parameters α and β are determined by curve fitting the finite element results. For the quasi-isotropic laminates being considered in the present study, the above interpolating function has been successfully fitted to the 2-D scarf joint ($\alpha = 0.435$, $\beta = 0.116$) and the 3-D scarf repair results ($\alpha = 0.618$, $\beta = 0.297$), as shown in Figure 22. One advantage of the use of rational function is that the maximum shear strain can be readily expressed in terms of the average shear stress,

$$\frac{\gamma_{\max}}{\gamma_Y} = \frac{\alpha}{1 - \tau_{av}/\tau_Y} - \beta, \tag{5}$$

To design a scarf joint or scarf repair to avoid failures of the adhesive bond, it is important to ensure the maximum adhesive shear strain remain below the adhesive failure strain γ_F, i.e.,

$$\gamma_{\max} \le \gamma_F . \tag{6}$$

In this case, the highest average shear stress that the adhesive bond can sustain is given by,

$$\tau_{av} = \tau_Y g(\gamma_F / \gamma_Y). \tag{7}$$

Consequently the maximum scarf angle that can restore a damaged composite laminate to its design ultimate strain (ε_{DUS}), without failure of the adhesive bond, can be expressed as, noting the average shear stress is related to the applied load via equation (1),

$$\theta = \frac{1}{2}\sin^{-1}\left(\frac{2\tau_Y g(\gamma_F/\gamma_Y)}{E\,\varepsilon_{DUS}}\right). \tag{8}$$

The above expression furnishes an improved solution of the appropriate scarf angle necessary to restore the strength of a damaged composite laminate to its as-designed ultimate strain (ε_{DUS}).

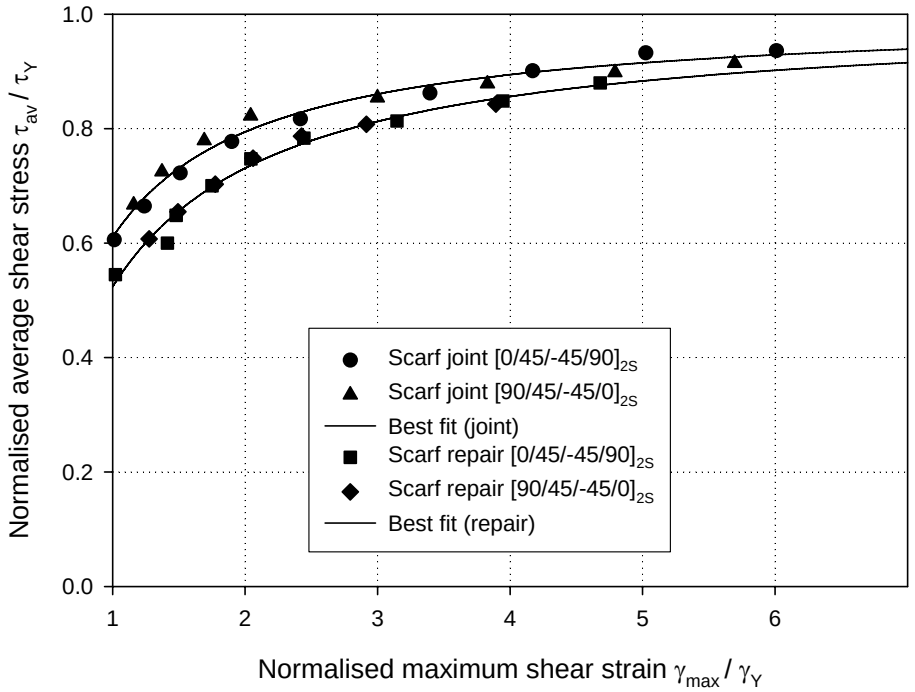

Figure 22 Average shear stress versus maximum shear strain at the highest load location. Symbols indicate FE results

It should be pointed out that the parameters α and β need to be determined for every stacking sequence or joint geometry (taking into account other factors such the presence of external doublers or local defects). However, it is possible to determine an upper bound solution that would yield a conservative prediction of repair efficiency. This approach would then provide a simple method to include the effects of strain concentrations and adhesive plasticity in the analysis of scarf repairs to composite structures.

The above first order predictive model does not account for the variations found in the experimental results (Figure 11), due to the non-uniform deformation through the bondline thickness, as evidenced in the finite element results shown in Figure 12. Stress concentrations away from the adhesive centreline resulted in over-prediction of the joint strength for 0-0 and 0-90 joints. To further improve the predictive method, the function $g(\gamma_F / \gamma_Y)$ must also account for the non-uniform distribution of the shear strain within the adhesive, not just along the adhesive centreline. Unfortunately, this is a more complex task because the peak strains associated with singularities are mesh-dependant. It is possible to account for this effect by employing the 'characteristic distance' approach, or a fracture-mechanics based approach. However, such a methodology would complicate the analysis and require further investigation to determine exactly how large the 'characteristic distance' must be. Other factors may also come into consideration, such as the adhesive thickness, tip bluntness, and local variations in scarf angle.

A further complicating factor is that the peak strains determined in this analysis were all calculated assuming a scarf angle of 5°. Previous parametric studies based on linear analysis have shown that the scarf angle, laminate thickness and adhesive thickness may all influence the stress distribution along the adhesive centre line [9]. Depending on the sensitivity of α and β to these variables, an iterative solution may be required to achieve convergence when designing a scarf repair to consider all of these variations to scarf joint geometry. Further investigation of these influencing factors is required, particularly in the presence of adhesive plasticity.

7. Conclusions

The strength of scarf repairs in composite structures has been thoroughly investigated. It has been shown, by both analysis and experiment, that the stacking sequence of composite adherends influences the scarf joint strength. This influence is due to the fact that the adhesive shear stress distribution along the scarf is not constant. Local variations in adherend stiffness, corresponding to changes in ply orientation, result in peak shear and peel stresses in the adhesive far above the uniformly-distributed values often assumed in simple joint analyses. Hence, it can be concluded that the assumption of constant shear stress and peel stress can only be reasonably applied for isotropic adherends, i.e. metallic structures.

An improved joint analysis has been developed, which accounts for the effect of stiffness variation of composite adherends. Comparison with experimental results confirmed that the new approach provides a good prediction of joint strength when the load-bearing fibres (0°) are away from the laminate surface. It has been shown by analysis that peak local stresses arise at stress concentrations around the termination of 0° plies, away from the adhesive centreline. This effect has caused some over-prediction of joint strength where load-bearing fibres (0°) are at the laminate surface. Further work is required to improve the joint strength analysis methodology.

Acknowledgement: the authors would like to thank Dr. Alan Baker and Prof. I. Herszberg for helpful discussions. This work has been carried out as part of a joint task between DSTO and CRC-ACS.

8. References

1. RAAF, *DEF(AUST)9005 Issue A: Composite Materials and Adhesive Bonded Repairs*. 2005
2. Hart-Smith, L.J., *Adhesively-bonded scarf and stepped-lap joints*. 1973, NASA Technical Report CR 112237
3. Baker, A.A., *Joining and repair of aircraft composite structures.* Mechanical Engineering Transactions, 1996. **ME21**(No. 1 & 2): p. 1-59.
4. Oplinger, D.W., *Mechanical fastening and adhesive bonding*, in *Handbook of composites*, S.T. Peters, Editor. 1998, Chapman& Hall: London. p. 610-666.
5. Lubkin, J.L., *A theory of adhesive scarf joints*. Journal of Applied Mechanics, 1956. **July 1957**: p. 255-260.
6. Erdogan, F. and Ratwani, M., *Stress distribution in bonded joints.* Journal of Composite Materials, 1971. **5**: p. 378-393.
7. Baker, A.A., Chester, R.J., Hugo, G.R., and Radtke, T.C., *Scarf repairs to highly strained graphite/epoxy structure.* International Journal of Adhesion and Adhesives, 1999. **19**: p. 161-171.
8. Harman, A. and Wang, C.H. *Analytic and finite element stress predictions in two dimensional scarf joints*. in *Australian and International Aerospace Conference*. 2005. Melbourne, Australia.
9. Gunnion, A.J. and Herszberg, I., *Parametric study of scarf joints in composite structures.* Composite Structures, 2006. **75**: p. 364–376.
10. Soutis, C. and Hu, F.Z., *Strength analysis of adhesively bonded repairs*, in *Recent Advances in Structural Joints and Repairs for Composite Materials*, L.T.a.C. Soutic, Editor. 2003, Kluwer Academic Publishers: Longon. p. 141-170.
11. Trabocco, R.E., Donnellan, T.M., and Williams, J.G., *Repair of composite aircraft*, in *Bonded repair of aircraft structures*, A.A.a.J. Baker, R., Editor. 1988, Martinus Nijhoff Publishers: Dordrecht. p. 175-209.
12. Rubin, A.M., *Qualification of 121C (250F) curing adhesive for F/A-18 bonded repairs*. 1996, McDonnell Douglas Aerospace, MDC 96A0109
13. Rubin, A.M. *Secondary bonded composite joint analysis methodology update*. in *12th International Composite Repair Engineering Development (CREDP) Program Meeting*. 1996. St Louis: McDonnell Douglas Aerspace.
14. Harman, A., *Testing of Thick Adherend Bonded Scarf Joint 2D Test Coupons*. 2005, CRC-ACS TM 05046
15. Gorden, K., *FM300 High Shear Strength Modified Epoxy Adhesive*. 2002, Cytect Engineered Materials
16. Cytec, *FM300-2 modified epoxy resin film*. 1998, Cytec Engineered Materials
17. Whitney, J.M. and Nuismer, R.J., *Stress fracture criteria for laminated composites containing stress concentrations.* Journal of Composite Materials, 1974. **8**: p. 253-265.
18. Gosse, J. *Strain invariant failure criteria for fiber reinforced polymeric composite materials*. in *Proceedings of 13th ICCM conference*. 2001. Beijing, China.
19. Wang, C.H., *Progress multi-scale modelling of composite laminates*, in *Multi-scale modelling of composite material systems*, C.S.a.P.W.R. Beaumont, Editor. 2005, Woodhed Publishing: Cambridge. p. 259-277.

20. Soni, S.R. and Pagano, N.J., *Elastic response of composite laminates*, in *Mechanics of composite materials: recent advances*, Z. Hashin and C.T. Herakovich, Editors. 1983: Blacksburg, VA. p. 227-242.
21. Tsai, H.C., Alper, J., and Barrett, D. *Failure analysis of composite bonded joints*. in *AIAA/ASME/ASCE/AHS/ASC Structures, Structural Dynamics, and Materials Conference and Exhibit, 41st*. 2000. Atlanta, GA; UNITED STATES.
22. Pipes, R.B., Adkins, D.W., and Deaton, J., *Strength and repair of bonded scarf joints for repair of composite materials*. 1982, NASA Langley Research Center, MSG 1304
23. Dutton, S. and Baker, A.A., *Aircraft Applications and Design Issues*, in *Composite Materials for Aircraft Structures*, J.A. Schetz, Editor. 2004, American Institute of Aeronautics and Astronautics: Reston VA. p. 435 – 475.

Appendix A: Generalised plane strain method

When modeling large composite monolithic structures, each ply is typically treated as a 2-D orthotropic material within a laminate, the axial and bending stiffness of which can be determined using laminate theory. The resulting stiffness is then assigned to a shell element under the assumption of plane stress. With this approach, it is not possible to model a scarf joint for the purposes of determining the local stress-strain behaviour in the adhesive. Instead, either a full 3-D local model must be used or a 2-D solid element model that assumes either plane strain (simulating a biaxial loading state or generalized plane strain (constant, non-zero strain in the shell thickness direction, e.g., a laminate subjected to uniaxial loading). These assumptions are illustrated in Figure A.1.

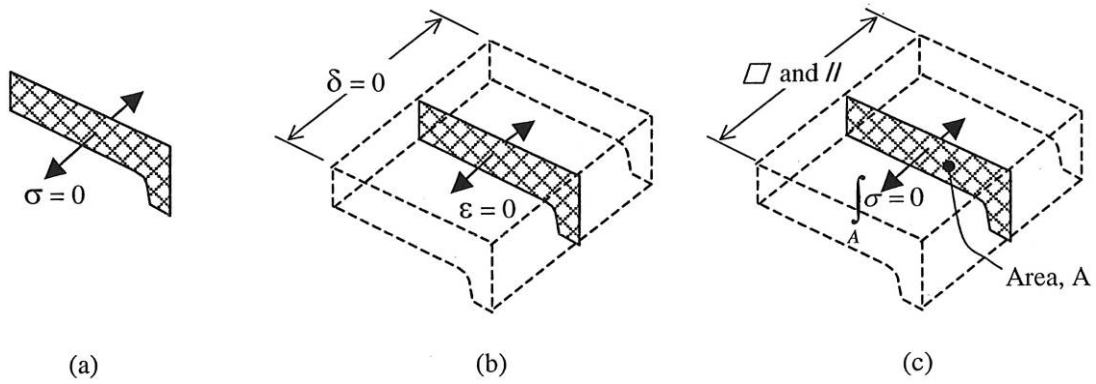

Figure A1: (a) plane stress, (b) plane strain, (c) generalised plane strain (after Reference (A.1))

To model a scarf joint specimen of finite width (25 mm), the most efficient method is to use a generalised plane strain model. This model formulation is three-dimensional, thus requiring appropriate material properties to be assigned to the elements. The required three-dimensional orthotropic material properties can be determined from the ply properties, by assuming the through-thickness properties are equal to transverse values (each ply is considered to be transversely isotropic with respect to the fibre direction). The 3-D orthotropic material properties for Cycom 970/T300 12K material, which has been used in the experiments and the finite element modeling, are given in Table A.1.

The material properties in Table A.1 can be directly applied to the 0^o plies in the generalized-plane strain model with reference to a coordinate system with the x-axis in the 0^o direction and the y-axis in the laminate thickness direction (in the element plane). The z-axis represents the width direction (normal to the element plane). Unique 3-D materials were defined for each ply orientation and assigned to each property set with respect to the same coordinate system. Hence, the 90^o ply material was also 3-D orthotropic and identical to that in Table A.1, except with the fibre direction stiffness now attributed to the width direction (z). This is represented in Table A.2. The off-axis plies require a 3-D anisotropic material model to properly represent their stiffness. The 3-D orthotropic properties for the +/- 45^o plies were obtained using the matrix transformation method [A.2]; the values are listed Table A.3.

Table A.1 3-D Three-dimensional orthotropic material properties for 0º plies

Property	**Value**
E_1 (MPa)	120000
$E_2 = E_3$ (MPa)	8000
$\nu_{12}=\nu_{12}$	0.3
ν_{23}	0.45
$G_{12} = G_{13}$ (MPa)	5000
G_{23} (MPa)	2760

Table A.2 Three-dimensional orthotropic material properties for 90º plies

Property	**Value**
$E_1 = E_2$ (MPa)	8000
E_3 (MPa)	120000
ν_{12}	0.45
ν_{23}	0.02
ν_{31}	0.3
G_{12} (MPa)	2760
$G_{23} = G_{31}$ (MPa)	5000

The stresses and strains in the local system, denoted by subscripts 1, 2 and 3 are given by

$$\begin{bmatrix}\sigma_1\\ \sigma_2\\ \sigma_3\\ \tau_{12}\\ \tau_{31}\\ \tau_{23}\end{bmatrix} = \begin{bmatrix} C_{11} & C_{12} & C_{12} & 0 & 0 & 0\\ C_{12} & C_{22} & C_{23} & 0 & 0 & 0\\ C_{13} & C_{23} & C_{33} & 0 & 0 & 0\\ 0 & 0 & 0 & C_{55} & 0 & 0\\ 0 & 0 & 0 & 0 & C_{55} & 0\\ 0 & 0 & 0 & 0 & 0 & \dfrac{C_{22}-C_{23}}{2}\end{bmatrix}\begin{bmatrix}\varepsilon_1\\ \varepsilon_2\\ \varepsilon_3\\ \gamma_{12}\\ \gamma_{31}\\ \gamma_{23}\end{bmatrix}, \tag{A.1}$$

or, in short,

$$\{\sigma_{1,2,3}\} = [C]\{\varepsilon_{1,2,3}\}. \tag{A2}$$

The stiffness matrix [C] is the inverse of the compliance matrix [S], i.e., $[C]=[S]^{-1}$. The terms of the compliance matrix are expressed in terms of the engineering constants as given below:

$$S_{11} = 1/E_1 \tag{A3a}$$
$$S_{12} = -\nu_{12}/E_1 \tag{A3b}$$
$$S_{13} = -\nu_{13}/E_1 \tag{A3c}$$
$$S_{22} = 1/E_2 \tag{A3d}$$
$$S_{23} = -\nu_{23}/E_2 \tag{A3e}$$
$$S_{33} = 1/E_3 \tag{A3f}$$

$$S_{55} = 1/G_{12} \quad \text{(A3g)}$$

$$S_{66} = 1/G_{23} \quad \text{(A3h)}$$

For a global coordinate system, whose y-axis is in the through-thickness direction of the laminate, and the x-axis is at angle θ to the fibre direction, the stresses and strains are related by the transformed stiffness matrix, as follows,

$$\{\sigma_{x,y,z}\} = [\overline{C}]\{\varepsilon_{x,y,z}\}, \quad \text{(A.4)}$$

where $[\overline{C}]$ is given by

$$[\overline{C}] = [T^{-1}][C][T^{-T}], \quad \text{(A.5)}$$

with the transformation matrix T being given by

$$[T] = \begin{bmatrix} \cos^2\theta & 0 & \sin^2\theta & 0 & -2\sin\theta\cos\theta & 0 \\ 0 & 1 & 0 & 0 & 0 & 0 \\ \sin^2\theta & 0 & \cos^2\theta & 0 & 2\sin\theta\cos\theta & 0 \\ 0 & 0 & 0 & \cos\theta & 0 & -\sin\theta \\ \sin\theta\cos\theta & 0 & -\sin\theta\cos\theta & 0 & \cos^2\theta - \sin^2\theta & 0 \\ 0 & 0 & 0 & \sin\theta & 0 & \cos\theta \end{bmatrix} \quad \text{(A.6)}$$

Table A.3 Three-dimensional orthotropic material properties for 45º plies [- 45º plies]

Property	**Value**	**Property**	**Value**
C_{11}	40448	C_{41}	0
C_{12}	4569	C_{42}	0
C_{13}	30448	C_{43}	0
C_{14}	0	C_{44}	3880
C_{15}	-28121 [+28121]	C_{45}	0
C_{16}	0	C_{46}	-1120 [+1120]
C_{21}	4569	C_{51}	-28121 [+28121]
C_{22}	10194	C_{52}	108 [-108]
C_{23}	4569	C_{53}	-28121 [+28121]
C_{24}	0	C_{54}	0
C_{25}	108	C_{55}	30987
C_{26}	0	C_{56}	0
C_{31}	30448	C_{61}	0
C_{32}	4569	C_{62}	0
C_{33}	40448	C_{63}	0
C_{34}	0	C_{64}	-1120 [+1120]
C_{35}	-28121 [+28121]	C_{65}	0
C_{36}	0	C_{66}	3880

References:

[A.1] Feih, S., Design of Composite Adhesive Joints, PhD Thesis, Cambridge University, March 2002.

[A.2] Dickerson, T., Components are three-dimensional but…, Advanced Workbook of Examples and Case Studies, Volume 2, Issue 2, NAFEMS Ltd, 2004.

DISTRIBUTION LIST
Design Methodology for Scarf Repairs to Composite Structures

C. H. Wang and A. Gunnion

AUSTRALIA

DEFENCE ORGANISATION	**No. of copies**
Task Sponsor	
DGTA	1 Printed
S&T Program	
Chief Defence Scientist	1
Deputy Chief Defence Scientist Policy	1
AS Science Corporate Management	1
Director General Science Policy Development	1
Counsellor Defence Science, London	Doc Data Sheet
Counsellor Defence Science, Washington	Doc Data Sheet
Scientific Adviser to MRDC, Thailand	Doc Data Sheet
Scientific Adviser Joint	Doc Data Sht & Dist List
Navy Scientific Adviser	Doc Data Sht & Dist List
Scientific Adviser – Army	Doc Data Sht & Dist List
Air Force Scientific Adviser	Doc Data Sht & Dist List
Scientific Adviser to the DMO	Doc Data Sht & Dist List
Deputy Chief Defence Scientist Platform and Human Systems	Doc Data Sht & Exec Summary
Chief of Air Vehicles Division	Doc Data Sht & Dist List
Research Leader	Doc Data Sht & Dist List
Head	1
Task Manager	1
Chun Wang	1 Printed
A. Gunnion	1 Printed
DSTO Library and Archives	
Library Fishermans Bend	Doc Data Sheet
Library Edinburgh	1 printed
Defence Archives	1 printed
Capability Development Group	
Director General Maritime Development	Doc Data Sheet
Director General Land Development	1
Director General Capability and Plans	Doc Data Sheet
Assistant Secretary Investment Analysis	Doc Data Sheet
Director Capability Plans and Programming	Doc Data Sheet

Chief Information Officer Group

Head Information Capability Management Division	Doc Data Sheet
Director General Australian Defence Simulation Office	Doc Data Sheet
AS Information Strategy and Futures	Doc Data Sheet
Director General Information Services	Doc Data Sheet

Strategy Group

Assistant Secretary Strategic Planning	Doc Data Sheet
Assistant Secretary International and Domestic Security Policy	Doc Data Sheet

Navy

Maritime Operational Analysis Centre, Building 89/90 Garden Island Sydney NSW Deputy Director (Operations) Deputy Director (Analysis)	Doc Data Sht & Dist List
Director General Navy Capability, Performance and Plans, Navy Headquarters	Doc Data Sheet
Director General Navy Strategic Policy and Futures, Navy Headquarters	Doc Data Sheet

Air Force

SO (Science) - Headquarters Air Combat Group, RAAF Base, Williamtown NSW 2314	Doc Data Sht & Exec Summary
Staff Officer Science Surveillance and Response Group	Doc Data Sht & Exec Summary

Army

ABCA National Standardisation Officer Land Warfare Development Sector, Puckapunyal	e-mailed Doc Data Sheet
J86 (TCS GROUP), DJFHQ	Doc Data Sheet
SO (Science) - Land Headquarters (LHQ), Victoria Barracks NSW	Doc Data Sht & Exec Summary
SO (Science) - Special Operations Command (SOCOMD), R5-SB-15, Russell Offices Canberra	Doc Data Sht & Exec Summary
SO (Science), Deployable Joint Force Headquarters (DJFHQ) (L), Enoggera QLD	Doc Data Sheet

Joint Operations Command

Director General Joint Operations	Doc Data Sheet
Chief of Staff Headquarters Joint Operations Command	Doc Data Sheet
Commandant ADF Warfare Centre	Doc Data Sheet
Director General Strategic Logistics	Doc Data Sheet

Intelligence and Security Group

AS Concepts, Capability and Resources	1
DGSTA , Defence Intelligence Organisation	1
Manager, Information Centre, Defence Intelligence Organisation	1
Director Advanced Capabilities	Doc Data Sheet

Defence Materiel Organisation

Deputy CEO	Doc Data Sheet
Head Aerospace Systems Division	Doc Data Sheet
Head Maritime Systems Division	Doc Data Sheet
Program Manager Air Warfare Destroyer	Doc Data Sheet
Guided Weapon & Explosive Ordnance Branch (GWEO)	Doc Data Sheet
CDR Joint Logistics Command	Doc Data Sheet

OTHER ORGANISATIONS

National Library of Australia	1
NASA (Canberra)	1

UNIVERSITIES AND COLLEGES

Australian Defence Force Academy

Library	1
Head of Aerospace and Mechanical Engineering	1
Hargrave Library, Monash University	Doc Data Sheet

OUTSIDE AUSTRALIA

INTERNATIONAL DEFENCE INFORMATION CENTRES

US Defense Technical Information Center	1
UK Dstl Knowledge Services	1
Canada Defence Research Directorate R&D Knowledge & Information Management (DRDKIM)	1
NZ Defence Information Centre	1

ABSTRACTING AND INFORMATION ORGANISATIONS

Library, Chemical Abstracts Reference Service	1
Engineering Societies Library, US	1
Materials Information, Cambridge Scientific Abstracts, US	1
Documents Librarian, The Center for Research Libraries, US	1

SPARES	5 Printed

Total number of copies: 30 Printed: 10 PDF: 20

DEFENCE SCIENCE AND TECHNOLOGY ORGANISATION
DOCUMENT CONTROL DATA

1. PRIVACY MARKING/CAVEAT (OF DOCUMENT)

2. TITLE

Design Methodology for Scarf Repairs to Composite Structures

3. SECURITY CLASSIFICATION (FOR UNCLASSIFIED REPORTS THAT ARE LIMITED RELEASE USE (L) NEXT TO DOCUMENT CLASSIFICATION)

Document	(U)
Title	(U)
Abstract	(U)

4. AUTHOR(S)

C. H. Wang and A. Gunnion

5. CORPORATE AUTHOR

DSTO Defence Science and Technology Organisation
506 Lorimer St
Fishermans Bend Victoria 3207 Australia

6a. DSTO NUMBER	6b. AR NUMBER	6c. TYPE OF REPORT	7. DOCUMENT DATE
DSTO-RR-0317	AR-013-718	Research Report	August 2006

8. FILE NUMBER	9. TASK NUMBER	10. TASK SPONSOR	11. NO. OF PAGES	12. NO. OF REFERENCES
2006/1111869/1	AIR 04/241	DGTA	32	23

13. URL on the World Wide Web

http://www.dsto.defence.gov.au/corporate/reports/DSTO-RR-0317 .pdf

14. RELEASE AUTHORITY

Chief, Air Vehicles Division

15. SECONDARY RELEASE STATEMENT OF THIS DOCUMENT

Approved for public release

OVERSEAS ENQUIRIES OUTSIDE STATED LIMITATIONS SHOULD BE REFERRED THROUGH DOCUMENT EXCHANGE, PO BOX 1500, EDINBURGH, SA 5111

16. DELIBERATE ANNOUNCEMENT

No Limitations

17. CITATION IN OTHER DOCUMENTS Yes

18. DSTO Research Library Thesaurus

Bonded repair, Failure theory, composite, scarf repair

19. ABSTRACT

Scarf repairs are the preferred method of repairing thick composite structures, especially when externally bonded patches can no longer meet the stiffness, strength, and flushness requirements. Present designs of scarf repairs are based on two-dimensional analyses of scarf joints, assuming a uniform stress distribution along the scarf. This report presents an improve design methodology for designing scarf repairs to composite laminates. With the aid of elastic-plastic analyses, a critical assessment of the current design methods has been carried out, with major emphasis being placed on the stress/strain concentration along the bondline. It is proposed to replace the shear stress criterion with the maximum strain criterion. Comparison with experimental results confirmed that the new approach provides an improved first-order prediction of repair efficiency of scarf repairs.